Nuclear Materials and Energy 19 (2019) 72–78

Contents lists available at ScienceDirect

Nuclear Materials and Energy

journal homepage: www.elsevier.com/locate/nme

Comparing N versus Ne as divertor radiators in ASDEX-upgrade and ITER

Elizaveta Sytova[a,b,c,d,e,*], Richard A. Pitts[a], Elizaveta Kaveeva[c], Xavier Bonnin[a], David Coster[b], Vladimir Rozhansky[c], Ilya Senichenkov[c], Irina Veselova[c], Sergey Voskoboynikov[c], Felix Reimold[f]

[a] ITER Organization, Route de Vinon-sur-Verdon, CS 90 046, 13067 St. Paul Lez Durance Cedex, France
[b] Max-Planck Institute for Plasma Physics, D-85748 Garching, Germany
[c] Peter the Great St. Petersburg Polytechnic University, 195251 St. Petersburg, Russia
[d] Ghent University, Department of Applied physics, Ghent, Belgium
[e] Aix-Marseille Universite, Ecole Doctorale Physique et Sciences de la Matiere, Marseille, France
[f] Max-Planck Institute for Plasma Physics, D-17491 Greifswald, Germany

A B S T R A C T

The study aims to estimate the influence of machine scale size on the behavior of plasma with extrinsic seeded impurities in the scrape-off layer (SOL) and divertor. This is performed through the comparison of plasma boundary simulations using the SOLPS-ITER code including drifts and currents of nitrogen (N) and neon (Ne) injection in ITER and ASDEX Upgrade (AUG) geometries. Trends are examined between the two seeding species in each individual device and by a comparison of the differences between the two machines. In the modeling results, the radiated power peak is located near the X-point in the inner divertor for the AUG cases and in the vicinity of the strike points in both divertors in ITER. The simulations also find less Ne impurity ions in the divertor volume than N and more significant Ne radiation inside the separatrix for AUG, consistent with published experimental findings. In ITER, both species radiate mostly from the divertor, in agreement with the existing SOLPS-4.3 simulation database obtained without drifts and with a less sophisticated treatment of parallel impurity transport. Drifts are important players in determining the plasma background for AUG and are comparatively less important in ITER. In both devices, the spatial distribution of the impurity ion density is complex, with their parallel flow patterns correlating with the thermal and friction force balance. Within this isolated modeling study, the principal reasons for different behavior between N and Ne on AUG and ITER appear to be the combination of a stronger drift effect and reduced screening of recycled fuel and impurity from divertor to private flux region on AUG leading to a more extended, colder plasma than in ITER. The increased temperature in the confined region just inside the separatrix on ITER also means that impurity ions reaching this zone are fully ionized and do not contribute significantly to the radiation loss there. On the basis of this study, both N and Ne are found to be acceptable low Z radiators on ITER.

1. Introduction

To remain below technologically acceptable stationary power loads on its tungsten (W) targets, ITER will require partially detached divertor operation obtained by the use of impurity seeding during burning plasma operation [1]. As a consequence of operation close to the H-mode power transition threshold ($P_{sep}/P_{LH} \sim 2$), it is currently expected that ITER will use the low Z extrinsic radiators, nitrogen (N) and neon (Ne), since higher Z impurity will almost certainly lead to excessive core radiation losses. Experiments on current all-metal wall devices (e.g. ASDEX-Upgrade (AUG) and JET) [2], however, indicate that there are important differences between the two species in terms of impurity transport. Nitrogen is generally observed to be more efficiently compressed than Ne, providing more localized divertor radiation. In contrast, simulations for ITER at high performance [3] indicate that compression will be similar. The fully recycling (lack of surface chemistry) nature of Ne makes it more attractive as a divertor radiator on ITER. When injected into tokamaks with tungsten armored divertors, N is known to lead to the formation of ammonia [4] which, in the case of deuterium-tritium operation in ITER, will produce tritiated ammonia, impacting both the treatment of exhaust gases and the machine duty cycle through the additional overhead on cryopump regeneration.

This paper presents the first results from a comparison of SOLPS-ITER plasma boundary simulations of the ITER and AUG divertors with N and Ne seeding and including fluid drifts. This purely numerical study aims in particular to identify the impact of scale size on the efficiency of divertor impurity retention. In the case of the AUG simulations, the modeling uses the real machine geometry and an experimentally obtained magnetic equilibrium, but does not attempt to match plasma measurements in any specific plasma discharge. It follows closely a study [5] performed with an older version of the SOLPS code, but deploys the most recent version of SOLPS-ITER (v.3.0.6) incorporating a more accurate treatment of impurity ions [6].

* Corresponding author.
E-mail address: elizaveta.sytova@ipp.mpg.de (E. Sytova).

https://doi.org/10.1016/j.nme.2019.02.019
Received 5 December 2018; Accepted 14 February 2019
Available online 23 February 2019

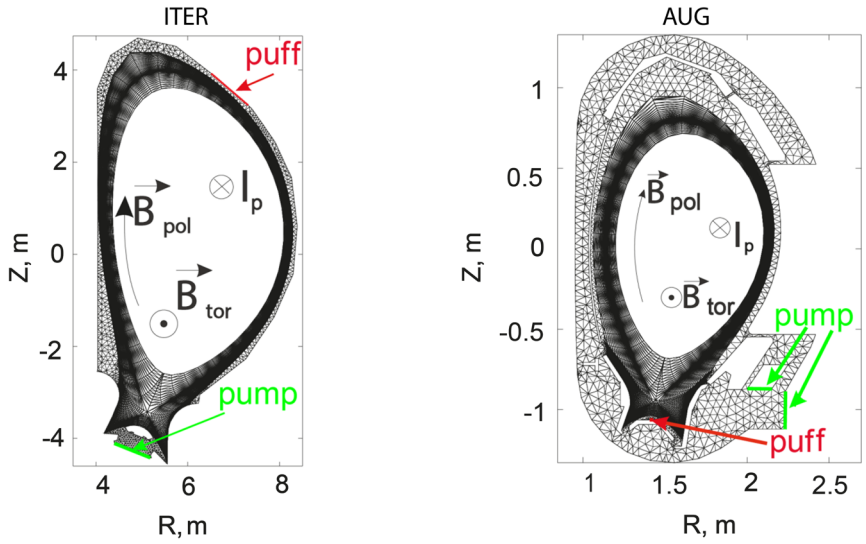

Fig. 1. Computational mesh for ITER (left) and AUG cases (right).

2. Modeling setup

For this SOLPS-ITER computational study, numerical meshes (Fig. 1) were selected as follows: for the ITER cases, the standard (F57) mesh was assumed [1,3], corresponding to a $q_{95} = 3$ burning plasma (H-mode) magnetic equilibrium ($I_p = 15$ MA, $B_T = 5.3$ T); for AUG the grid was created based on the real machine geometry and the equilibrium corresponding to the Type I ELMing H-mode shot #28903 [7,8], with $I_p = 800$ kA, $B_T = 2.5$ T and with higher $q_{95} = 5.5$ than for the ITER cases. Note again that no serious attempt is made here to match experimental results – the study is comparative and aims to compare the use of different seeding gases on a large (reactor scale) and medium-sized tokamak. The ITER simulations include beryllium as wall material and tungsten (W) on the divertor contour, with W assumed on all wall and divertor surfaces for AUG. In both cases (AUG and ITER) neither Be nor W sputtering is activated and W impurity is not followed in the calculations.

Radial transport is not modeled self-consistently in the SOLPS-ITER code, in common with all boundary plasma simulation packages of this type, and is instead always specified as an input parameter. Anomalous radial transport coefficients for particles ($D_\perp$) and heat ($\chi_\perp$) used in the present study are shown in Fig. 2. They differ between the different machines, but remain the same within each geometry for the two seeding species considered. To mimic the H-mode transport barrier, $D_\perp$ and heat $\chi_\perp$ are reduced in the core region in both cases, though the structure for the AUG cases, based on [11], is more complex and is intended to provide similar outboard midplane pedestal/SOL profiles to those seen in experiment for pulse #28903.

Key input parameters for the simulations are compared in Table 1. In particular, injected powers of $P_{in} = 100$ MW and 5 MW at the inner core boundary of the numerical grid for ITER and AUG respectively, noting that the power is distributed equally between ions and electrons for ITER, but not for AUG where, as noted above, the different profiles for $\chi_{\perp i}$ and $\chi_{\perp e}$ are selected to match upstream profile measurements even though no attempt is made here to compare the code predictions in the divertor with experiment. For AUG 1.8 MW and 3.2 MW are carried in the ion and electron channels respectively. Naturally, given the difference in scale size, the absolute quantities of fuel (deuterium) and seeded impurities are very much larger for ITER than AUG, but the ratios of impurity to fuel input are similar for the two machines for Ne and at least comparable for N. As shown later (see Table 2), the rates were also chosen to try and approximately match the total radiated power fractions between the devices for each given seed impurity.

The poloidal velocity of the main ions at the core boundary is set in

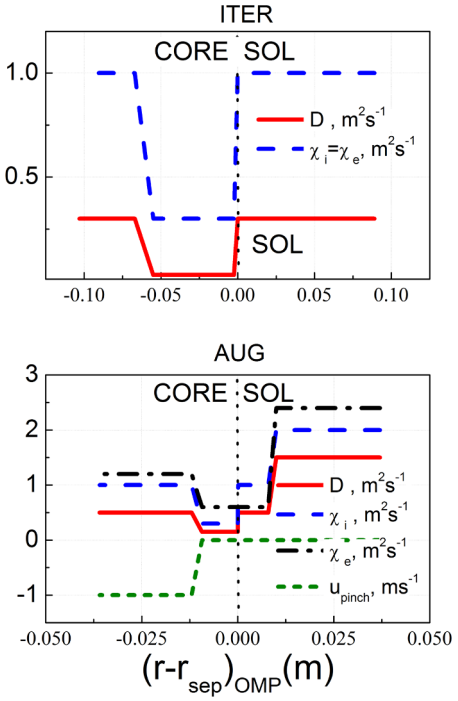

Fig. 2. Profiles of radial transport coefficients for ITER (left) and AUG geometry (right) simulations.

Table 1
Key parameters of the AUG and ITER model cases. $s_{||}$ is the parallel distance along the field line from target to target for the flux tubes just outside the separatrix ($(r - r_{sep})_{omp} = 1.6$ mm for ITER case, $(r - r_{sep})_{omp} = 0.35$ mm for AUG).

	ITER		AUG	
q_{95}	3		5.5	
$s_{||}$ (m)	190		130	
P_{in} (MW)	100		5	
D_{puff} (10^{23} e/s)	1.95		0.2	
Seeded gas	N	Ne	N	Ne
Seeding rate (10^{21} e/s)	21	2	0.35	0.2
Seeding/fuel ratio (%)	11	1	1.8	1
Neutral pressure (Pa)	11.4	11.6	9.7	9.3

Table 2
Radiated power fractions (normalized to P_{in}) and absolute radiated powers (in parentheses) for the four regions of the computational domain. $P_{rad,div}$ is the total radiated power below the X-point.

	P_{rad_tot}/P_{in};P_{rad_tot} (MW)	$P_{rad\_div}/P_{in}P_{rad,div}$ (MW)	$P_{rad\_SOL}/P_{in}P_{rad,SOL}$ (MW)	$P_{rad\_CORE}/P_{in}P_{rad,core}$ (MW)
ITER N	0.6 (60)	0.53 (53)	0.05 (5.3)	0.02 (2)
ITER Ne	0.67 (67)	0.53 (53)	0.085 (8.5)	0.05 (5)
AUG N	0.48 (2.4)	0.33 (1.6)	0.12 (0.61)	0.03 (0.15)
AUG Ne	0.52 (2.6)	0.23 (1.18)	0.16 (0.84)	0.13 (0.56)

such a way that the Mach number, M = 0.2 for AUG (accounting for the injected torque from neutral beam injection (NBI)) and M = 0 for ITER (where NBI torque is negligible). Boundary conditions at the targets were set to sheath boundary conditions for all variables (electron and ion temperatures, ion densities and poloidal velocities, electric potential [7]). Decay length boundary conditions are specified at the main wall and the PFR (private flux region) boundaries.

As shown in Fig. 1, impurities are injected into the ITER simulation grid from the same location (upper lateral port) as that used in the main ITER SOLPS-4.3 simulation database [1,3]. In the case of AUG, injection is through the divertor dome structure, as in experiment. A more comparable study would have been to inject impurities/fuel also into the ITER subdivertor volume, as is now likely to be the case in reality for divertor detachment control when ITER operates, but the choice of an upper lateral injection is historical since, as mentioned, this is the location which has been chosen for the vast majority of ITER simulations to date. Using the same injection point as in previous studies allows the new SOLPS-ITER drift runs presented here to be directly compared with older SOLPS-4.3 cases without drifts. Comparative simulations with divertor injection are underway.

3. Key modeling results

Fig. 3 compiles the outer midplane (OMP) profiles of T_e and n_e for the 4 model cases (ITER, AUG, N, Ne) demonstrating a good match throughout the profile for the two seeding species in each of the two devices. The effect of the reduced anomalous transport coefficients in the region just inside the separatrix can be clearly seen. This choice of cross-field transport yields OMP near-SOL values of $\lambda_q \sim 4$ mm (ITER) and $\lambda_q \sim 1.4$ mm (AUG) where λ_q is the characteristic width of parallel heat flux density. The value for AUG used in the modeling is roughly consistent with the expectations of the multi-machine empirical scaling for attached, inter-ELM H-mode conditions [9]. Divertor neutral pressure values, averaged on the private flux region boundary of the

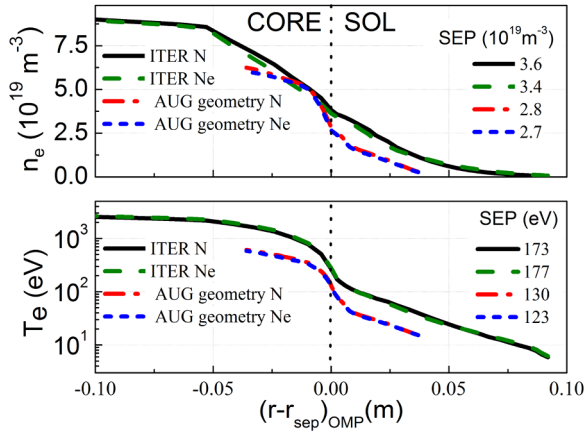

Fig. 3. Outer midplane T_e and n_e radial profiles for the 4 model cases (AUG and ITER, N and Ne seeding). Values of the separatrix are listed explicitly.

computational domain are ~11.5 Pa for ITER cases and ~9.5 Pa for AUG cases. The distributions of n_e and T_e in the divertor for all 4 simulation cases are compared in Figs. 4 and 5 respectively, with Fig. 6 showing the corresponding inner and outer target power flux densities (assuming cylindrically symmetric targets). The figures illustrate very

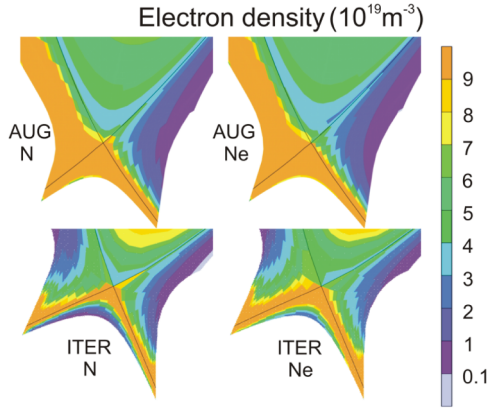

Fig. 4. 2D distributions of divertor plasma electron density for the 4 model cases.

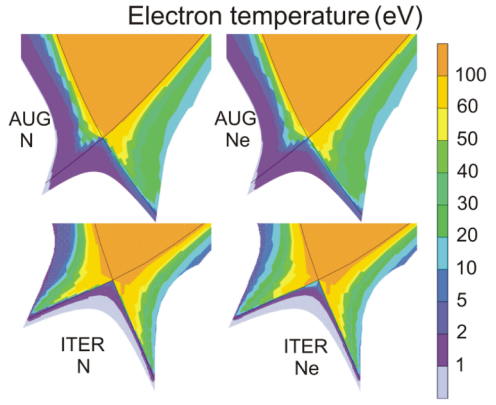

Fig. 5. 2D distributions of divertor plasma electron temperature for the 4 model cases.

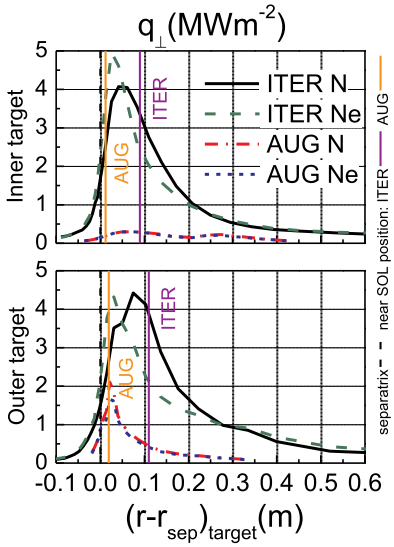

Fig. 6. Power flux density profiles at inner (left) and outer (right) targets for the 4 model cases. The vertical lines mark the extent of the near-SOL (fluxed tubes close to separatrix projected onto the target): 9 mm and 11 mm at the inner and outer targets respectively for ITER and 1.2 mm and 1.9 mm for AUG.

sharply the differences between the large and small scales for comparable relative levels of impurity injection. In AUG, for both N and Ne as extrinsic radiators, the simulations feature an extended cold and dense region (similar to 'high field side high density' (HFSHD) phenomenon, seen in experiment [10]) near the inner divertor target with low target power flux density, clearly indicating a fully detached state. In contrast, the outer target is in a partially detached state [14], with low T_e only in the strike point vicinity and much more peaked power flux density profiles.

The ITER cases are essentially symmetric with respect to target in-out power density, independently of seeded impurity, and are partially detached at both targets. As discussed in [11], the key drivers for the observed behavior in the AUG simulations are ExB drifts; when these drifts are deactivated the strongly detached, HFSHD region in the inner divertor leg is greatly reduced and the target loading is more symmetric. The absence of strong asymmetry in the ITER cases is an indication for a weaker effect of drifts (see Section 3.1). To zero order this is expected given the relative difference in toroidal magnetic field strength between the two devices (5.3 T cf. 2.5 T). Separate code runs for ITER without drifts activated (not shown here) produce similar results to those shown in Figs. 4–6, confirming the relatively low drift impact. In addition, the radiation distributions found in simulations within the main ITER divertor design simulation database obtained with the SOLPS-4.3 code (which does not include a drift model) are very similar to these SOLPS-ITER cases for equivalent divertor conditions (e.g. sub-divertor neutral pressure and impurity concentration) [1].

A further important consequence of the difference in scale size between AUG and ITER is the larger parallel distance between the X-point and the strong temperature gradient and strong ionization region in the divertor (at least for flux tubes near the separatrix), see Figs. 5 and 9. It is this region of high temperature gradient which separates the cold detached zone from upstream locations. In addition, not only is this distance larger on ITER, but the absolute value of T_e is considerably higher than on AUG, meaning that a given ionization state of the seeded impurity will exist at different physical locations in the divertor. The stronger impact of drifts on AUG further exacerbates the situation by leading to the formation of a HFSHD region, decreasing again the distance from X-point to ionization front.

3.1. The role of ExB drifts

Due to the complexity and nonlinearity of the system, the comparative role of drifts in edge plasmas of different machines can be determined quantitatively only by modeling. The main consequence of drifts in AUG is the redistribution of plasma between the divertor targets driven by flows through the PFR. This redistribution leads to many consequences, which evolve self-consistently, and can be traced in modeling. The degree of detachment of the inner divertor increases, improving impurity retention and leading to a higher impurity concentration there and subsequent amplification of the divertor asymmetry through an increased radiation asymmetry. The decrease of electric conductivity due to the reduced plasma temperature in the inner divertor leads to a qualitative change in electrostatic potential and drifts – the electric field in a detached divertor is determined by the balance of the electric force and electron-ion friction, so that the potential is not of a Boltzmann type for electrons. Though based on different modeling conditions to those described here, more details can be found in [11,12].

To yield the chain of events listed above, the ExB drifts must redistribute a considerable fraction of the plasma ionized in the process of divertor recycling. The relative importance of drifts thus depends on the ratio two quantities: (1) the flux of ions Γ_{ExB} dragged by drifts across the separatrix below the X-point towards the PFR, then further along the equipotential lines in PFR towards the inner divertor, and (2) the flux of particles ionized in the outer divertor and returned to the plate by parallel flow, $\Gamma_{||}$. The former may be estimated as $\Gamma_{ExB} = 2\pi R \cdot n_i \cdot v_{ExB} \approx 2\pi R \cdot n_i \cdot L_x E_{pol}/B \rightarrow \Gamma_{ExB} = 2\pi R L_x \cdot n_i \cdot E_{pol}/B$ and the latter as $\Gamma_{||} = 2\pi R \cdot n_i \cdot c_s \cdot L_r \cdot \frac{B_{pol}}{B}$ with R the major radius, L_x the poloidal distance along the separatrix over which the poloidal electric field is significant, n_i the ion density, L_r the width of the divertor SOL in physical space for density and heat flow (which can be assumed $\cong \lambda_q$ for the purposes of this approximate argument), c_s the sound speed and B_{pol} the poloidal magnetic field.

The product $L_x \cdot E_{pol}$ is simply the potential drop in the divertor, from X-point to the plate. For the conduction limited or partially detached regime it can be approximated as $L_x \cdot E_{pol} \approx T_{eX}/e$ with $T_{e,X}$ the electron temperature at the X-point. In the outer divertor, the ExB to parallel flux density ratio is thus

$$\Gamma_{ExB}/\Gamma_{||} = T_{eX}/(ec_s B_{pol} L_r) \quad (1)$$

Concerning parameter L_r, the choice of cross-field transport coefficients in the near SOL being comparable but not identical for the two simulation sets (AUG and ITER, see Fig. 2), the different geometries of the machines lead both to the OMP SOL and divertor SOL widths about 3–4 times larger for ITER than AUG in this modelling study. This is clearly seen in energy distributions along the plates for AUG and ITER, Fig. 6— the SOL width for energy flow is bigger for ITER. The value of B_{pol} is about 4 times higher on ITER than on AUG (1.3 T vs. 0.34 T at the OMP and 0.7 T vs. 0.13 T) at the outer strike point). Plasma temperatures at the X-point are also higher on ITER than on AUG (Fig. 7), though the difference is only approximately a factor 1.5. The same also applies at the OMP (Fig. 3). The temperature behaviour can be

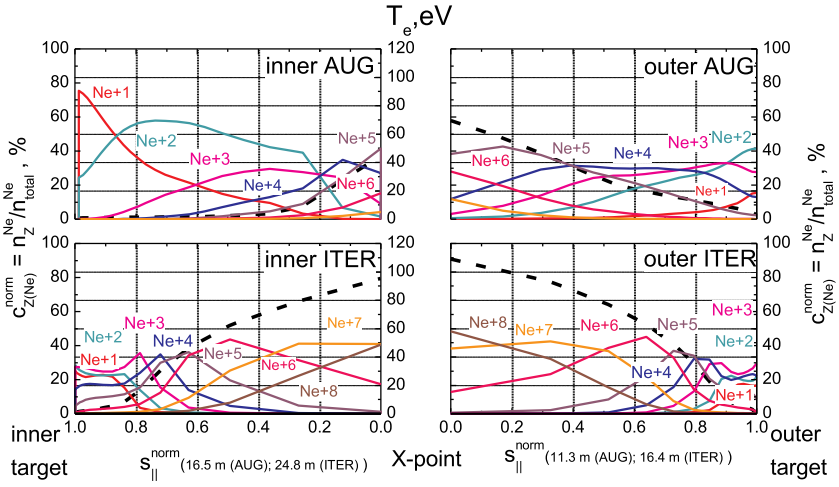

Fig. 7. Parallel T_e profiles along SOL flux tubes close to the separatrix ($(r - r_{sep})_{omp} = 1.6$ mm for ITER case, $(r - r_{sep})_{omp} = 0.35$ mm for AUG). The parallel distance, $s_{||}$ is normalized to unity, with $s_{||} = 1$ at the targets and $s_{||} = 0$ at the X-point. The variation of the fractional density (in %) of the different Ne charge states (normalized to the total Ne density) is also marked.

explained, qualitatively, by the fact that in the semi-detached region of the divertor plasma, T_e is low, of order 1–2 eV so that the temperature drop between divertor and upstream regions is determined to zero order by electron heat conductivity: $T_{e\,X} \sim (L_{||}q_{||})^{2/7}$, where $L_{||}$ is a parallel distance between the cold ionisation front and the upstream location and $q_{||}$ the parallel heat flow density. The latter scales roughly as $q_{||} \sim P_{SOL}/(R\lambda_q(B_{pol}/B)_{OMP})$being comparable between the two devices in the case of this simulation study. A slightly higher temperature in ITER in the present modeling setup is therefore expected due to the larger value of $L_{||}$ from the X-point to the divertor, but the 2/7 power means that the difference will be small, particularly since (see Fig. 7) the larger value of q_{95} on AUG leads to comparable values of $L_{||}$ as on ITER despite the much smaller machine size. For example the connection length for at $(r - r_{sep})_{OMP} = 10$ mm for ITER from the X-point to the outer plate is 17 m while for a geometrically approximately similar tube at $(r - r_{sep})_{OMP} = 3$ mm in the AUG case, the same connection length is 10 m. The fact that the values of T_{eX} are so much higher on ITER than AUG is a reflection of the importance of two dimensional effects and convective energy transport, both of which are fully captured by the modeling.

By far the largest difference between the two devices with regard to the flux ratio in Eq. (1) is the product of $B_{pol}L_r$, which is a factor ~10–15 higher on ITER than on AUG so that within the context of the simulations reported here and the simple arguments leading to Eq. (1), the impact of drifts would be expected to be lower on ITER, as observed. It is important to point out, however, that if the radial heat transport in the ITER simulation had been reduced so as to be consistent with the current best experimental scaling [9] of the near SOL heat flux width (λ_q α $1/B_{pol}$ ~ 1 mm for ITER at 15 MA), the arguments given above would point to a stronger effect of drifts in ITER. Drift simulations for ITER similar to those presented here but with reduced transport are planned.

3.2. Temperature redistribution and impurity radiation

Very different temperature distributions in the divertor area of AUG and ITER are strongly connected to the different impurity ionization state distributions, and hence different radiation distributions, though it is hard to extract, even from the modeling results, which is the driver and which is the consequence. Focusing on Ne only (a similar picture applies to the case of N-seeding but is not shown here for brevity) Fig. 7 illustrates the Ne charge state distributions for the two machines along the inner and outer divertor near SOL flux tubes, together with the corresponding T_e profiles. Tables 2 and 3 complement Fig. 7, giving various radiated power fractions (normalized to P_{in}) as well as the absolute values of power radiated in the core, main SOL and divertor regions (Table 2) and the fractional power (normalized to the total in the divertor) radiated by the various N and Ne charge states (Table 3).

In the case of AUG, most of the divertor radiation originates from charge states Ne^{3+}-Ne^{5+} which are spread along the divertor legs towards the X-point. In ITER, divertor radiation is much more strongly localized near the targets and comes principally from charge states Ne^{3+}-Ne^{6+}. In this simulation study, the ITER divertor thus remains hotter, leading to increased ionization to higher charge states of the impurities as they travel up along the divertor leg towards the X-point.

Table 3
Radiated power fractions (as a percentage of the total radiated power) in the divertor region due to the different impurity charge states for N and Ne.

	Ne^{+1}-Ne^{+2}	Ne^{+3}	Ne^{+4}	Ne^{+5}	Ne^{+6}	Ne^{+7}-Ne^{+10}
AUG	15.7	20.2	30	20.9	7.1	2.1
ITER	8.4	18.2	22.3	23.4	23.1	4.6
	N^{+1}	N^{+2}	N^{+3}	N^{+4}	N^{+5}-N^{+7}	
AUG	12	19	28	33	8	
ITER	14	25	29	28	4	

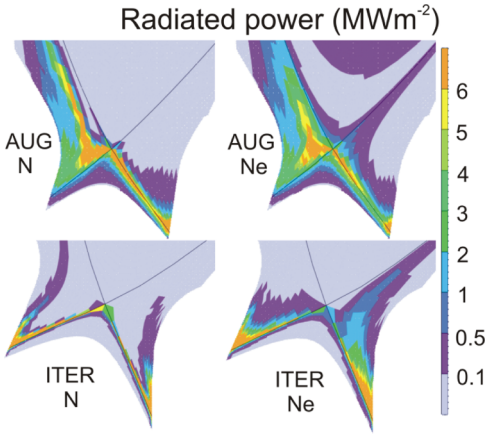

Fig. 8. 2D distributions of radiated power in the divertor region for the 4 model cases.

In turn this reduces the radiation in the X-point vicinity and keeps the plasma temperature high through much of the divertor. In AUG the divertor is colder, leading to more efficient radiation in the X-point vicinity, pulling T_e down further. These differences can be readily seen in the total radiated power distributions in Fig. 8. In the case of N seeding, the T_e in AUG is sufficient for the most powerfully radiating charge states to be still localized in the divertor so that their relative contribution to the total divertor radiation is comparable in both AUG and ITER.

In addition to the effects which drifts may have in modifying the background plasma, there is another important feature of the simulation set described here which influences the plasma temperature and the distribution of impurities. In the vertical target geometry characterizing the AUG and ITER devices, neutral (fuel and impurity) atoms recycled from the targets are directed towards the separatrix and may migrate into the PFR with high probability depending on the ratio of the ionization mean-free-path to the divertor SOL width. Once in the PFR, impurities can access SOL flux tubes higher upstream. The ionization source distributions in Fig. 9 clearly show regions of strong ionization along the divertor separatrices with a much greater spatial extent relative to the SOL width for AUG than ITER. Moreover, the absence of strong ionization in the near SOL region at the target in ITER and the comparatively broad ionization zones on AUG clearly show that screening is more efficient in the ITER case, which has ~3x greater SOL width in comparison to the AUG model case for comparable $q_{||}$). A test of the screening hypothesis put forward here would require the transport to be reduced in ITER to produce a comparable divertor SOL width to that in AUG in the same way suggested in Section 3.1 concerning the drift impact.

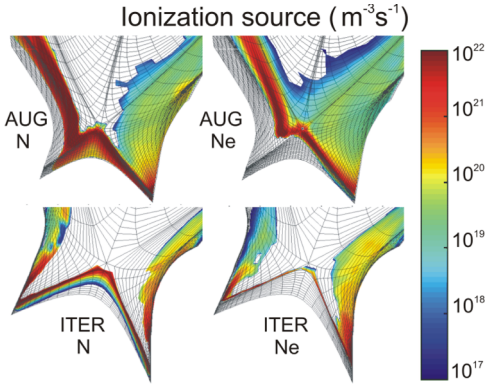

Fig. 9. 2D ionization source distributions for the 4 model cases.

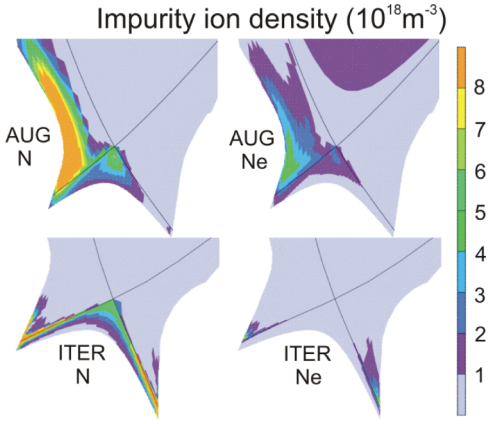

Fig. 10. 2D impurity density distributions (summed over all charged species) for the 4 model cases.

3.3. Impurity parallel transport patterns

It is generally observed in the simulations, for both AUG and ITER that the impurities are mostly concentrated in the cold plasma layers in the target vicinity (see the two-dimensional distributions of total impurity in densities in Fig. 10), while the radiation is found on the boundaries of these layers (Fig. 8). Nevertheless, the details of ionized impurity transport which determine the compression of impurities in the divertor are complex. This transport is being carefully examined using the simulations discussed in this paper and only a brief discussion of the some of the salient points is possible here.

As previously shown for AUG [13, 15], the parallel momentum balance equation for impurities is dominated by the friction and thermal forces, which are in balance. From this balance, assuming the parallel forces acting on impurity ions to be of the form $S_{||}^{Fr} \approx \alpha Z^2 \tau^{-1} n_I m_I (v_{||i} - v_{||I})$ for friction and $S_{||}^{Th} \approx \beta Z^2 n_I \nabla_{||} T_i$ for the thermal force, an approximate expression for the impurity parallel velocity can be written: $v_{||I} \approx v_{||i} + \frac{\beta}{\alpha} \tau m_I^{-1} \nabla_{||} T_i$, where $v_{||I}$ is the impurity parallel velocity, $v_{||i}$ the main ion parallel velocity, m_I the impurity ion mass, τ the collision time, n_i the main ion density, $\nabla_{||} T_i$ the parallel projection of main ion temperature gradient and α, β are numerical coefficients (dependent on impurity densities only for big impurity concentrations). This expression implies that the impurity parallel velocity is determined mostly by that of the main ions and that the only difference between the two velocities can be provided by the ion temperature gradient force. This statement remains true for both AUG and ITER simulations in this paper. Fig. 11 compares the near-SOL impurity and main ion parallel velocities showing that the impact of the thermal force (the difference between velocities) is larger in the ITER divertor and can in principle increase leakage. This applies to both N and Ne seeding.

For the AUG cases the analysis in [11] shows that the flow difference provided by the ion temperature gradient force is essentially negligible for both Ne and N and is therefore not the most important player governing impurity leakage from the divertor. Instead, this mechanism is provided by the interplay of the impurity flow stagnation point and the impurity ionization front. The former is to a large extent determined by the main ion flow stagnation point, which is in turn controlled by the position of the ionization front of the main ions. The conclusion in [10] is thus that if the impurity ionization front is located closer to the target than that of the main ions, this impurity will be mostly retained. If it is located further away it will mostly leak upstream pushed by the reversed main ion flows. Since Ne has higher first ionization energy (21.6 eV) than N (14.5 eV), these arguments imply that poorer divertor retention is expected for Ne compared with N, consistent with modeling results. In fact, in AUG, this type of leakage is present only from the outer target, since the inner divertor target is fully detached and there is no reversed flow of the main ions upstream to push impurities from the divertor.

For the ITER case, Fig. 11 shows that there are larger differences between the velocities of the impurity and main ions due to thermal force produced mainly by ion temperature gradient which pushes the stagnation point of impurities towards the divertor and which is unfavorable for impurity retention for both impurities and both inner and outer divertors. This is unlike AUG where impurity flow reversal only occurs for Ne and only at the outer divertor. The higher T_e in ITER nevertheless still means that impurities ionize closer to the target, which improves retention. The interplay of these two factors leads to a similar outcome for ITER as seen in the AUG simulations but with clear quantitative differences: Ne is found to be less well retained than N, the main factor influencing the different retentions of the impurities being the difference in the positions of their ionization fronts. This is clearly seen in the radiated power distributions of Fig. 8 and the impurity ion densities in Fig. 10. As mentioned earlier in Section 3.2, however, even if Ne is marginally less well compressed in ITER, the larger divertor volume, and higher temperatures mean that most of the radiation still occurs in the divertor whilst the higher pedestal temperature on ITER means that Ne escaping to the core cannot radiate effectively there.

In connection with the impurity retention, a further interesting

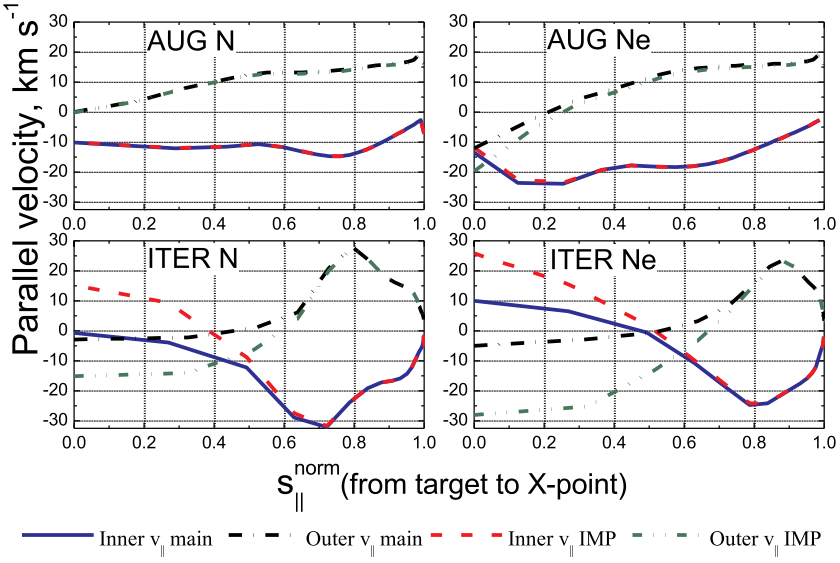

Fig. 11. Main ion (solid) and impurity ion (dashed) parallel velocity profiles along the normalized parallel distance s|| for the flux tubes as specified at Fig. 7 at both inner and outer divertors for the AUG and ITER Ne seeded model cases.

observation from these simulations is that very similar radiated power fractions can be achieved with comparable seeding to fueling ratios for both impurity species in AUG, whilst in ITER a much higher ratio of impurity to gas puff (~ factor 6) is required for N than Ne (see Table 1). The precise reasons for this different behavior at the two different size scales are not presently completely understood and are being further investigated.

4. Summary

A first attempt has been made to analyze the influence of machine scale on the behavior of plasma with low Z (neon and nitrogen) extrinsic seeded impurities in the scrape-off layer (SOL) and divertor by comparing simulations of AUG and ITER using SOLPS-ITER modeling with all drifts and currents activated. In the AUG case, the real geometry and an experimentally obtained plasma equilibrium is used, but with no serious attempt to benchmark against experiment. Seeding rates were chosen in each case to approximately match the radiated fractions between the two devices and to ensure a dissipative, partially detached divertor operating point for the ITER case, chosen to be consistent with the power exhaust expected for a Q = 10 burning plasma. Both simulations include H-mode pedestal regions inside the separatrix. The simulations find a pronounced in-out divertor asymmetry on AUG, featuring a dense plasma region on the high field side, similar to experimental observation. In the ITER case, the divertor plasma is much more symmetric and remains hotter over a much larger region below the X-point. These differences in plasma background are to zero order driven by the much more significant private flux region drift flows found in the AUG case. The ITER drift cases give very similar results to those from the main (SOLPS-4.3) ITER simulation database which does not feature drift capability, further confirming the lower impact of drifts on ITER solutions.

Radiation in the modeling results is found to be more localized in the divertor for ITER and extends up to the X-point in AUG, largely due to the very cold and dense inner divertor which leads to most of the seeded impurity being localized there. Higher plasma temperatures in the ITER case mean that the most powerfully radiating charge states are situated spatially closer to the targets. Any impurity which does escape into the main SOL and thence inside the separatrix is fully stripped thanks to the higher pedestal temperatures and cannot contribute to radiation losses. On AUG, Ne reaching the confined region is not fully stripped and can radiate more strongly.

Impurity transport in the SOL is analyzed in terms of the parallel momentum balance and its impact on the impurity velocity. The component of impurity leakage due to this parallel transport is the same in both of the simulation cases (AUG and ITER) and is dominated by upstream main ion frictional drag on the impurity with a secondary contribution from the ion temperature gradient which is only sizeable in ITER. In AUG it is found that N and Ne change the main ion flow (through their radiation characteristics) so that the impurity outflow from the outer divertor occurs only for Ne, while for ITER this occurs for the two divertors and the two impurities. The mechanism of impurity leaking out of the divertor is, in addition, more efficient for Ne than N because it ionizes further from the target than main ions, while N ionizes closer to the target. However, even though Ne spreads more widely than N in ITER, the larger physical size of the divertor that moves away the impurity flow reversal point from the target and the high divertor plasma temperature means that the majority of ion charge states responsible for the bulk of the radiation remain within the divertor volume for both species.

The analysis presented here is only a first step in understanding the impurity transport mechanisms at play in the ITER divertor. Much more work is required to further elucidate the relative importance of drifts and parallel transport, requiring a great deal more scanning of parameters, a complex operation given the extremely computationally intensive nature of such simulations at the ITER scale. Nevertheless, based on this early study, it would appear that both Ne and N would be acceptable seeding impurity species on ITER.

Copyright

Acknowledgments

This research was supported by the Erasmus Mundus Fusion DC Grant and the Russian Scientific Foundation Grant No. 17-12-01020. Numerical calculations were partially performed in the Polytechnic SuperComputer Center at Peter the Great St. Petersburg Polytechnic University.

References

[1] R.A. Pitts, et al., “Physics basis for the ITER tungsten divertor.”, these proceedings – to be submitted to NME (2018).
[2] M. Bernert, et al., Nucl. Mater. Energy 12 (2017) 111–118, https://doi.org/10.1016/j.nme.2016.12.029.
[3] A.S. Kukushkin, et al., Fusion Eng. Des. 86 (2011) 2865, https://doi.org/10.1016/j.fusengdes.2011.06.009.
[4] E. Pawelec, J. Phys. Conf. Ser. 959 (2018), https://doi.org/10.1088/1742-6596/959/1/012009.
[5] F. Reimold, et al., Proc. 26th IAEA Fusion Energy Conf, 2016.
[6] E. Sytova, et al., Contrib. Plasma Phys. (2018) 1–7, https://doi.org/10.1002/ctpp.201700135.
[7] F. Reimold, et al., Nucl. Mater. Energy 12 (2017) 193–199.
[8] F. Reimold, et al., J. Nucl. Mater. 463 (2015) 128–134, https://doi.org/10.1016/j.jnucmat.2014.12.019.
[9] T. Eich, et al., Nucl. Fusion (2013) 53, https://doi.org/10.1088/0029-5515/53/9/093031.
[10] F. Reimold, et al., 12 (2017) 193–199. doi:10.1016/j.nme.2017.01.010.
[11] I. Senichenkov, Plasma Phys. Controlled Fusion (2019), https://doi.org/10.1088/1361-6587/ab04d0.
[12] V. Rozhansky, et al., Contrib. Plasma Phys. (2018) 540–546, https://doi.org/10.1002/ctpp.201700119.
[13] P.C. Stangeby, The Plasma Boundary of Magnetic Fusion Devices, in: P.C Stangeby (Ed.), Institute of Physics Pub., Bristol; Philadelphia, 2000Print.
[14] S.I. Krasheninnikov, et al., J. Plasma Phys. 83 (2017) 155830501, , https://doi.org/10.1017/S0022377817000654.
[15] E. Sytova, 43rd EPS Conf. on Plasma Physics Leuven, Belgium, 2016 July 4–8. ISBN: 2-914771-99-1 P1.054.